# Simulation Analysis and Experimental Evaluation of Tractive Performance of Pneumatic Tire on Granular Terrain Based on DEM-FEM

**Peng Yang, Mengyan Zang and Haiyang Zeng**

M. Zang (✉), School of Mechanical and Automotive Engineering, SCUT,
Guangzhou 510640, China
myzang@scut.edu.cn

**Keywords** DEM-FEM, Granular Terrain, Pneumatic Tire, Tractive Performance

**Abstract** A combined discrete-finite element method is proposed to simulate the interaction between pneumatic tire and granular terrain, where the spherical discrete element method is used for the granular terrain and the finite element method is used for the pneumatic tire. Then, based on the self-developed software CDFP, the tractive performance of the pneumatic tire on granular terrain at different slip rates are simulated. In order to verify the effectiveness of the simulation results, a soil bin test facility was developed. The results show that the simulated rim sinkage and gross tractive force are basically corresponded with the experimental results. Numerical examples have verify the effectiveness of the proposed discrete-finite element method in studying the interaction between pneumatic tire and granular terrain.

## 1 Introduction

In the study of tire-granular terrain interactions, the numerical methods have gained growing popularity than the experimental methods among researchers, because of their repeatability and can analyze interactions from a micro perspective. The finite element method (FEM) as the most popular numerical method, with a long history of development and having been applied in many engineering applications [1, 2]. Although FEM is efficient to solve continuum mechanics, but numerous obstacles to simulate particle flows. Meanwhile, the discrete element method (DEM) can be employed to simulate particle flows [3, 4]. Though the DEM is capable of capturing the large displacement of granular terrain, it is unable to describe continuous deformation of the pneumatic tire. To take full advantages of both DEM and FEM, the combined discrete-finite element method (DEM-FEM) has been proposed for tire-granular terrain interaction simulations, in which pneumatic tire is described by finite element (FE) and granular terrain is described by discrete element (DE).

Recently, the interaction simulation between tire and granular terrain by using DEM-FEM application has reported by many researchers. A notable work is shown by Nakashima et al. [5-7]. Not only use 2D DEM-FEM to analyze the tractive performance of wheel running on sand, but also real automobile tires with different tread patterns were studied in their works. Although the 2D DEM-FEM can be used to analyze the tractive performance of wheel, it is difficult to express the actual stress state of wheel. Hence, a 3D DEM-FEM method is necessary in this problem. In recent years, application of 3D DEM-FEM to tire-granular terrain interaction has also been attempted by Michael et al. [8], Horner et al. [9] and Recuero et al. [10]. It is worth mentioning that Zang's research group [11-13] has done substantial work on tire-sand interaction simulations using 3D DEM-FEM, with which they analyzed the tractive performance of rigid wheel and pneumatic deformed tire.

In this study, we mainly focus on the interaction simulation between pneumatic tire and granular terrain. The paper is structured as follows. The basic theories of DEM-FEM and contact detection algorithm are introduced in Section 2. The experimental facility is presented in Section 3. Subsequently, the numerical example of tire-granular terrain interaction is illustrated in detail in Section 4. In Section 5, the simulation results are compared with the experimental results. Finally, some conclusions are given in Section 6.

## 2 Basic Theories

### 2.1 Contact Forces Between DE and DE

The motions of the DE and the FE node are governed by the Newton's Second Law. Each DE has six degrees of freedom. In this study, the contact forces between DE and DE can be calculated on the basis of Hertz-Mindlin contact model [14]. As depicted in Figure 1: $O_i$ and $O_j$ are the mass center of $DE_i$ and $DE_j$, respectively; C represents the contact point between the $DE_i$ and $DE_j$; $v_i$ and $\omega_i$ are the linear velocity and angular velocity of $DE_i$; $v_j$ and $\omega_j$ are the linear velocity and angular velocity of $DE_j$; $\boldsymbol{X}_i$, $\boldsymbol{X}_j$ and $\boldsymbol{X}_c$ are the position vectors of $O_i$, $O_j$ and C, respectively.

In the calculation of contact forces between $DE_i$ and $DE_j$, the contact forces including normal force and tangential force, can be calculated by Eq. (1).

$$\boldsymbol{F} = \boldsymbol{F}_n + \boldsymbol{F}_t \tag{1}$$

$$\boldsymbol{F}_n = \boldsymbol{F}_{n,\mathrm{e}} + \boldsymbol{F}_{n,\mathrm{vis}} \tag{2}$$

$$\boldsymbol{F}_t = \begin{cases} \boldsymbol{F}_{t,\mathrm{e}} + \boldsymbol{F}_{t,\mathrm{vis}}, & \left|\boldsymbol{F}_t\right| < \mu\left|\boldsymbol{F}_n\right| \\ \mu\boldsymbol{F}_n, & \left|\boldsymbol{F}_t\right| \geq \mu\left|\boldsymbol{F}_n\right| \end{cases} \tag{3}$$

As shown in Eq. (2), the normal force $\boldsymbol{F}_n$ contains the normal spring force $\boldsymbol{F}_{n,e}$ and normal damping force $\boldsymbol{F}_{n,vis}$. In Eq. (3), where $\mu$ is the friction factor among the elements; $\boldsymbol{F}_{t,e}$ and $\boldsymbol{F}_{t,vis}$ are the tangential spring force and tangential damping force. Can be calculated by the following equations:

$$\boldsymbol{F}_{n,\mathrm{e}} = (4/3)\left(E_i E_j / \left(E_i\left(1-v_j^2\right) + E_j\left(1-v_i^2\right)\right)\right) R_{ij}^{1/2} \boldsymbol{h}^{3/2} \tag{4}$$

$$\boldsymbol{F}_{t,\mathrm{e}} = -(16/3)\left(G_i G_j / \left(G_i\left(2-v_j\right) + G_j\left(2-v_i\right)\right)\right) R_{ij}^{1/2} \left\|\boldsymbol{h}\right\|^{1/2} \boldsymbol{\sigma}_t \tag{5}$$

$$\boldsymbol{F}_{n,\mathrm{vis}} = -\gamma_n \left(\left(m_i m_j\right) / \left(m_i + m_j\right)\right) \boldsymbol{v}_n \tag{6}$$

$$\boldsymbol{F}_{t,\mathrm{vis}} = -\gamma_t \left(\left(m_i m_j\right) / \left(m_i + m_j\right)\right) \boldsymbol{v}_t \tag{7}$$

where $v_i$, $v_j$, $E_i$, $E_j$ are two Poisson's ratios and two Young's moduli of $DE_i$ and $DE_j$, respectively; $R_{ij} = R_i R_j / \left(R_i + R_j\right)$ is the equivalent radius; $G_i = E_i / \left(2\left(1+v_i\right)\right)$ and $G_j = E_j / \left(2\left(1+v_j\right)\right)$ are the equivalent elastic shear moduli of $DE_i$ and $DE_j$, respectively; $\boldsymbol{\sigma}_t = \int \boldsymbol{v}_t dt$ is the relative displacement in the tangential direction; $\boldsymbol{v}_n$, $\boldsymbol{v}_t$ are the normal and tangential relative velocities on the contact point; $\gamma_n$, $\gamma_t$ are the damping factors of normal and

tangential directions, respectively; $m_i$, $m_j$ are the mass of $DE_i$ and $DE_j$, respectively.

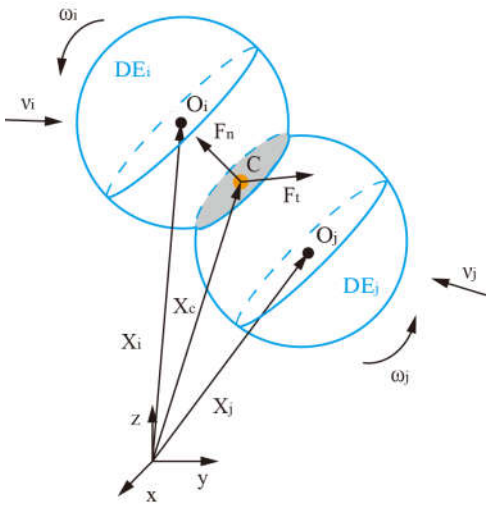


**Figure 1:** The DE-DE interaction model

## 2.2 Contact Forces Between DE and FE

As depicted in Figure 2: C represents the contact point between $DE_i$ and finite element segment $FE_j$; $O_i$ is the mass center of $DE_i$; $X_i$ and $X_c$ are the position vectors of $O_i$ and C, respectively; $v_i$ and $\omega_i$ are the linear velocity and angular velocity of $DE_i$; h is the depth of the overlap between $DE_i$ and $FE_j$. Here the $FE_j$ is treated as a sphere of infinite radius, then the contact forces between $DE_i$ and $FE_j$ can be calculated by the same equations as described in Sect. 2.1.

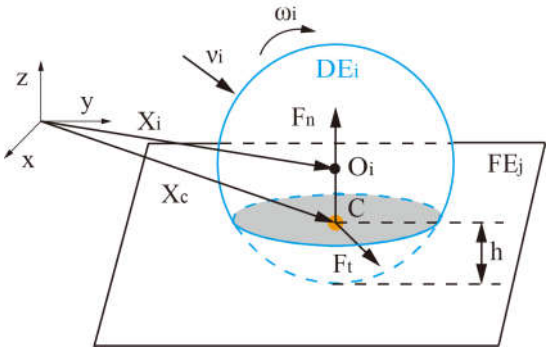


**Figure 2:** The DE-FE interaction model

## 2.3 Contact Algorithms

The contact detection of tire-granular terrain simulation model mainly involves two parts, i.e. the contact detection between discrete element and discrete element (DE-DE) and the contact detection between discrete element and finite element (DE-FE). In this work, the algorithm of CGRID [15] is used for contact detection of DE-DE. And the contact detection of DE-FE, we use the DZCell algorithm which we proposed in our previous work. For more details about the DZCell algorithm, readers can refer to the literature [16]. Then, the corresponding contact forces are calculated based on the Hertz-Mindlin model.

# 3 Experimental Facility

In order to obtain the tractive performance of pneumatic tire running on the granular terrain under different travel conditions, a soil bin test facility was developed. The soil bin

test facility is shown in Figure 3. The facility is mainly composed of three parts, i.e. the single wheel test device, the soil mixing/compaction device and the control system.

**Figure 3:** Soil bin test facility

The size of soil bin is 4000 × 650 × 400 $mm^3$. The soil bin is filled with the dry pebble particles. The diameters of the pebble particles range from 10 mm to 14 mm randomly. The tested tire nominal size is 37 × 12.5R16.5, with 890 mm in diameter and 310 mm in width, and the inflation pressure is 0.35 MPa.

## 4 Numerical Models

In this section, the tractive performance of pneumatic tire in interaction with granular terrain is simulated to validate the proposed DEM-FEM. The FEM is employed here for the pneumatic tire, whereas the granular terrain is represented by using DEM. The proposed DEM-FEM is implemented into an in-house developed code, CDFP (Combined Discrete-Finite Program).

### 4.1 The Model of the Tire

In this study, one pneumatic tire model is used for simulation analysis, which includes different layers and different material models. As shown in Figure 4(a), the size of the simulation tire is consistent with that of the experimental tire. The structure of the simulation tire is shown in Figure 4(b), including sidewall, carcass rubber, tread rubber, belt rubber, carcass reinforcement (shell), belt reinforcement (shell) and rim. The sidewall, carcass rubber, tread rubber and belt rubber are described by hexahedral finite elements, and the material is Mooney-Rivlin model. The carcass reinforcement and belt reinforcement are described by quadrilateral shell elements, and the material is orthotropic elastic model. The rim is defined as rigid. Material parameters are listed in Tables 1 and 2.

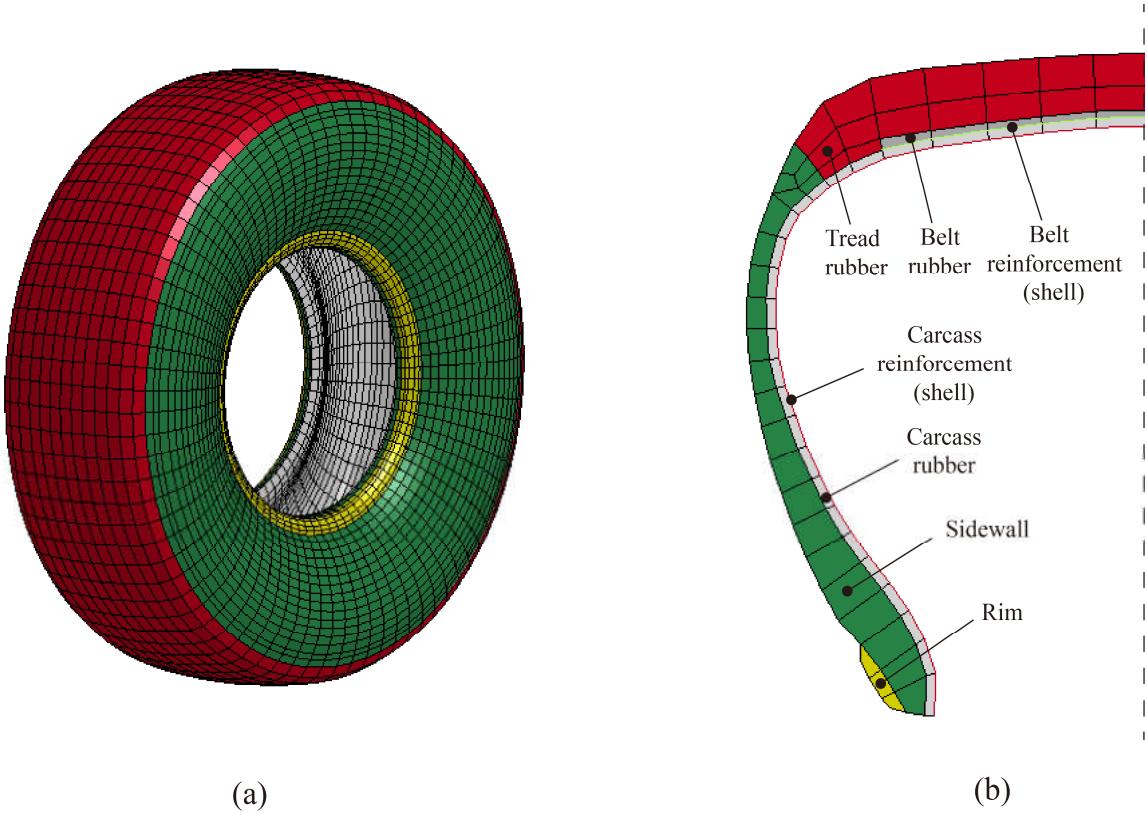


**Figure 4:** FE model of pneumatic tire: (a) tire model; (b) cross-sectional model

Table 1: Material parameters 1

| | Sidewall | Tread rubber | Carcass rubber | Belt rubber | Rim | Particle |
|---|---|---|---|---|---|---|
| A (MPa) | 1.12 | 1.12 | 1.82 | 1.12 | - | - |
| B (MPa) | 0.75 | 0.75 | 1.21 | 0.75 | - | - |
| Poisson's ratio | 0.49 | 0.49 | 0.49 | 0.49 | 0.28 | 0.2 |
| Density (kg/m$^3$) | $1.08 \times 10^3$ | $1.13 \times 10^3$ | $3.85 \times 10^3$ | $7.53 \times 10^3$ | $7.85 \times 10^3$ | $2.6 \times 10^3$ |
| Young's modulus (MPa) | - | - | - | - | $2.08 \times 10^5$ | $7.0 \times 10^4$ |

Table 2: Material parameters 2

| | Density (kg/m$^3$) | EA (MPa) | EB (MPa) | EC (MPa) | PRBA | PRCA | PRCB | GAB (MPa) | GBC (MPa) | GCA (MPa) |
|---|---|---|---|---|---|---|---|---|---|---|
| Belt reinforcement | $4.99\times10^3$ | 80641.06 | 57.49 | 57.49 | $2.67\times10^{-4}$ | $2.67\times10^{-4}$ | 0.49 | 13.99 | 19.29 | 13.99 |
| Carcass reinforcement | $1.14\times10^3$ | 22002.34 | 24.27 | 24.27 | $4.49\times10^{-4}$ | $4.49\times10^{-4}$ | 0.49 | 6.01 | 8.14 | 6.01 |

### 4.2 The Model of the Granular Terrain

As shown in Figure 5, the soil bin is used to simulate granular terrain. The size of soil bin is $2000 \times 650 \times 200$ mm$^3$, where the diameters of the particles range from 10 mm to 14 mm randomly, and the total number of particles is 142,390. A transparent wall is applied here as boundaries to prevent particles from penetrating the boundaries. The particles in the soil bin are stable after self-compaction. Contact parameters are listed in Table 3.

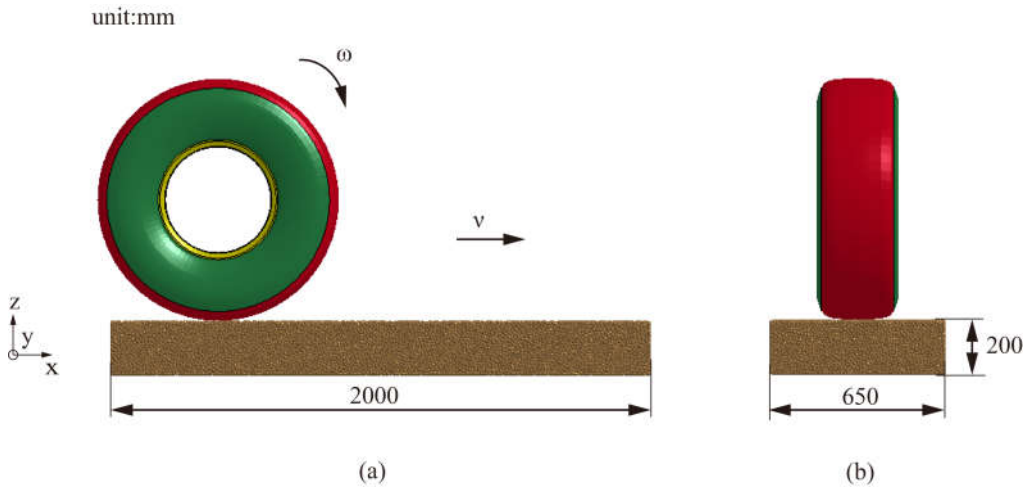


**Figure 5:** DEM-FEM model of tire-granular terrain interaction: (a) front view, (b) left view

Table 3: Contact parameters

| | Normal damping coefficient (1/s) | Tangential damping coefficient (1/s) | Friction coefficient |
|---|---|---|---|
| Tread-particle | 50 | 45 | 0.5 |
| Particle-particle | 50 | 45 | 0.4 |

### 4.3 Simulation Process

In Figure 5, the tire is coupled with the granular terrain. The time step is $3.0 \times 10^{-3}$ ms. The simulation process is as follows:

(1) Tire inflation: Tire pressure is 0.35 MPa. The pressure increases from 0 to 0.35 MPa in 0 to 10 ms.

(2) Force loading of the tire: The vertical load force is 9800 N, acting on the rim. The force increases from 10 to 12 ms.

(3) Velocity loading of the tire: The rotational velocity of the tire is fixed to be 2.247 rad/s. The tire under different slip conditions (10%, 20% and 30%) is simulated. Therefore, the translational velocity is changed with the slip. The translational and rotational velocities increase from 12 to 15 ms. Then, the tire is running normally.

## 5 Results and Discussion

Figure 6 shows the traveling track of the pneumatic tire, and the displacement contour of particles in the Z-direction is also shown. The granular terrain has significant displacement due to the interaction force of tire. As can be seen, displacement values are positive for particles on both sides of the trace, whereas, displacement values are negative for particles under the tire tread , which is consistent with real scenario.

Tractive forces are the results of shear forces generated in the contact patch that drive the pneumatic tire forward. These tractive forces are calculated as the summation of the interacting forces of all the particles in contact with the tire tread. As shown in Figure 7, the vertical reaction force of the pneumatic tire is maintained at a stable value during the movement.

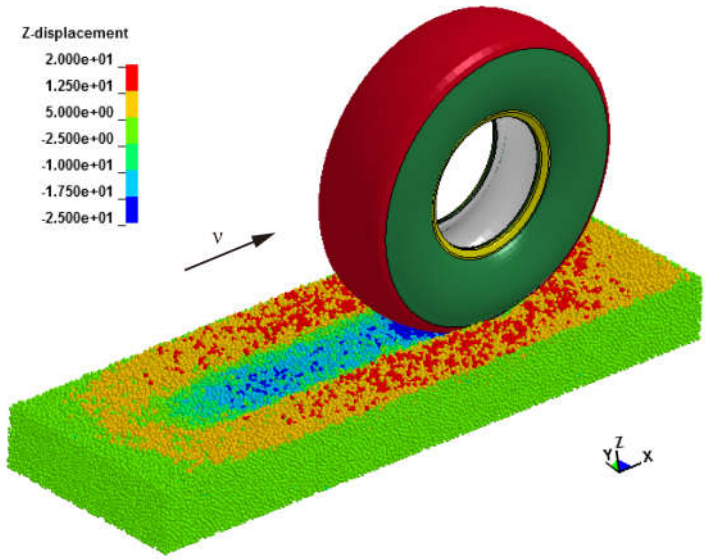


**Figure 6:** Z-displacement contour of the granular terrain

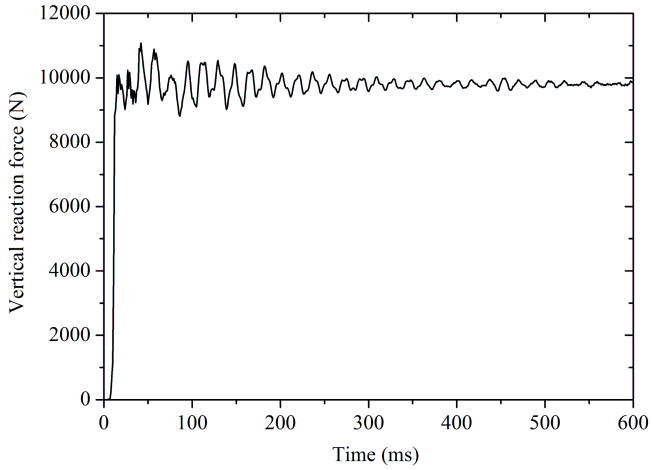


**Figure 7:** Time history of the vertical reaction force under the slip of 20%

Figures 8 and 9 show the simulation results of the pneumatic tire at different slip rates. In Figure 8, the rim sinkage rises along with the increase of slip rate. The simulation results are in good agreement with the experimental ones. In Figure 9, the gross tractive effort rises along with the increase of slip rate. This is because the granular terrain deformation in the traveling direction of the pneumatic tire increase with the slip rate, and the large terrain deformation causes the large gross tractive effort in turn. The trend of the simulation values is basically consistent with the experimental values.

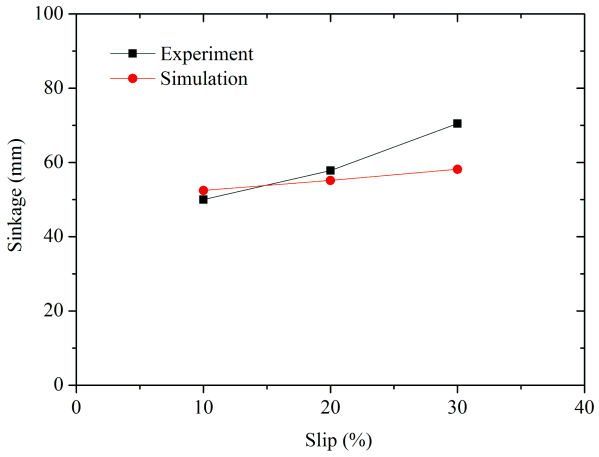


**Figure 8:** The rim sinkage versus the slip rate in the simulation

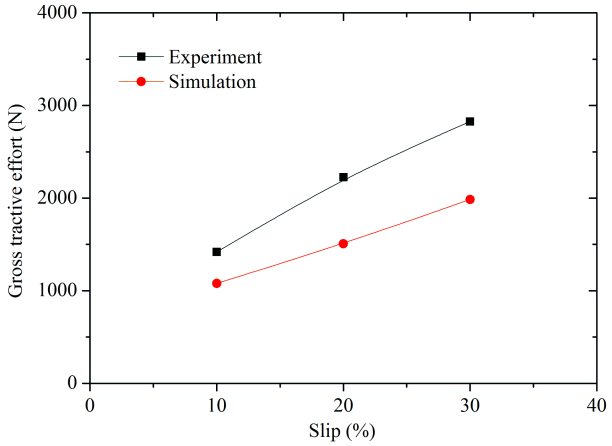


**Figure 9:** The gross tractive effort versus the slip rate in the simulation

## 6 Conclusions

A 3D combined discrete-finite element method is proposed to simulate the interaction between the pneumatic tire and granular terrain. The tractive performance of pneumatic tire, such as the normal reaction force, gross tractive effort and rim sinkage are simulated under different slip conditions by the proposed DEM-FEM. The results show that the simulated rim sinkage and gross tractive force are basically corresponded with the experimental results. Numerical examples have demonstrated the capacity of the proposed DEM-FEM to simulate the tire-granular terrain interactions.

## Acknowledgements

This work was supported by the National Key R&D Program of China (No. 2017YFE0117300), the Science and Technology Planning Project of Guangzhou (No. 201804020065), the National Natural Science Foundation of China (No. 11672344).

## References

[1] Rao, S. S. (2017). The finite element method in engineering. Butterworth-heinemann.

[2] Xia, K. (2011). Finite element modeling of tire/terrain interaction: Application to

predicting soil compaction and tire mobility. *Journal of Terramechanics* 48(2), 113-123.

[3] Naik, S., Malla, R., Shaw, M., & Chaudhuri, B. (2013). Investigation of comminution in a Wiley Mill: Experiments and DEM Simulations. *Powder technology* 237, 338-354.

[4] Alian, M., Ein-Mozaffari, F., & Upreti, S. R. (2015). Analysis of the mixing of solid particles in a plowshare mixer via discrete element method (DEM). *Powder technology* 274, 77-87.

[5] Nishiyama, K., Nakashima, H., Yoshida, T., Ono, T., Shimizu, H., Miyasaka, J., & Ohdoi, K. (2016). 2D FE–DEM analysis of tractive performance of an elastic wheel for planetary rovers. *Journal of Terramechanics* 64, 23-35.

[6] Nishiyama, K., Nakashima, H., Shimizu, H., Miyasaka, J., & Ohdoi, K. (2017). 2D FE–DEM analysis of contact stress and tractive performance of a tire driven on dry sand. *Journal of Terramechanics* 74, 25-33.

[7] Nishiyama, K., Nakashima, H., Yoshida, T., Shimizu, H., Miyasaka, J., & Ohdoi, K. (2018). FE-DEM with interchangeable modeling for off-road tire traction analysis. *Journal of Terramechanics* 78, 15-25.

[8] Michael, M., Vogel, F., & Peters, B. (2015). DEM–FEM coupling simulations of the interactions between a tire tread and granular terrain. *Computer Methods in Applied Mechanics and Engineering* 289, 227-248.

[9] Horner, D. A., Peters, J. F., & Carrillo, A. (2001). Large scale discrete element modeling of vehicle-soil interaction. *Journal of engineering mechanics* 127(10), 1027-1032.

[10] Recuero, A., Serban, R., Peterson, B., Sugiyama, H., Jayakumar, P., & Negrut, D. (2017). A high-fidelity approach for vehicle mobility simulation: Nonlinear finite element tires operating on granular material. *Journal of Terramechanics* 72, 39-54.

[11] Zhao, C., & Zang, M. (2014). Analysis of rigid tire traction performance on a sandy soil by 3D finite element–discrete element method. *Journal of Terramechanics* 55, 29-37.

[12] Zheng, Z., Zang, M., Chen, S., & Zeng, H. (2018). A GPU-based DEM-FEM computational framework for tire-sand interaction simulations. *Computers & Structures* 209, 74-92.

[13] Zhao, C. L., & Zang, M. Y. (2017). Application of the FEM/DEM and alternately moving road method to the simulation of tire-sand interactions. *Journal of Terramechanics* 72, 27-38.

[14] Balevičius, R., Džiugys, A., & Kačianauskas, R. (2004). Discrete element method and its application to the analysis of penetration into granular media. *Journal of Civil Engineering and Management* 10(1), 3-14.

[15] Williams, J. R., Perkins, E., & Cook, B. (2004). A contact algorithm for partitioning N arbitrary sized objects. *Engineering Computations* 21(2/3/4), 235-248.

[16] Zheng, Z., Zang, M., Chen, S., & Zhao, C. (2017). An improved 3D DEM-FEM contact detection algorithm for the interaction simulations between particles and structures. *Powder Technology* 305, 308-322.